ORIGINAL ARTICLE

Monte Carlo Simulation of Testicular Absorbed Dose in the Digimouse Phantom: Assessing the Impact of Organ Position and Surrounding Tissue Composition

Akbar Farhadi[1,2], Farhad Zolfagharpour[1*], Ahmet Bozkurt[3], Arash Abdolmaleki[4], Asadollah Asadid[5]

[1] *Department of Physics, Faculty of Science, University of Mohaghegh Ardabili, Ardabil, Iran*

[2] *Istanbul Technical University, Energy Institute, Division of Nuclear research, Istanbul, Turkiye*

[3] *Istanbul Technical University, Informatics Institute, Division of Computational Science and Engineering, Istanbul, Turkiye*

[4] *Department of Biophysics, Faculty of Advanced Technologies, University of Mohaghegh Ardabili, Namin, Iran*

[5] *Department of Biology, Faculty of Science, University of Mohaghegh Ardabili, Ardabil, Iran*

*Corresponding Author: Farhad Zolfagharpour

Email: Zolfagharpour@uma.ac.ir

Received: 03 December 2024 / Accepted: 15 February 2025

Abstract

Purpose: This article investigates the influence of testicular positioning and surrounding organ compositions on the absorbed dose in the testicles across a wide range of photon energies.

Materials and Methods: Using the Digimouse phantom in Geant4 with the mesh approach, the absorbed dose and deposited energy in mouse testicular tissue were calculated. Organ compositions followed ICRP Publication 145 guidelines. Four identical mono-energetic planar radiation sources (10 × 2.2 cm) emitting photons in the 2–10,000 keV range were positioned equidistantly around the mouse phantom at the head, tail, and both sides, 2 cm away, to ensure uniform irradiation. Simulations were conducted both with surrounding organs in anatomically accurate positions and with these organs replaced by air to assess their impact on dose distribution.

Results: Without surrounding organs, the absorbed dose was minimally influenced (<6%) by radiation source orientation. When surrounding organs were included, significant differences were observed, particularly at low photon energies (<25 keV), where notable radiation shielding occurred. Above 25 keV, adjacent organs increased energy deposition in testicular tissue due to secondary scattering, with absorbed dose differences between opposing orientations (e.g., head vs. tail) ranging from 30–92%. At 25 keV, surrounding organs did not affect energy deposition.

Conclusion: Surrounding organs significantly influence testicular absorbed dose, particularly at low photon energies where shielding dominates, and at higher energies where secondary scattering enhances deposition. These findings highlight the importance of considering organ interactions and source positioning in dosimetry to optimize radiation therapy protocols and reduce risks to sensitive organs.

Keywords: Monte Carlo Simulations; Testes Position; Energy Deposition; Absorbed Dose; Geant4.

DOI:

1. Introduction

Accurate dosimetry is essential in medical imaging and radiation therapy to assess radiation exposure and its potential biological effects on organs. The testicular tissue, in particular, is highly vulnerable to radiation damage, necessitating precise dosimetry to minimize the risk of potential harm. The complex anatomy and varying positions of organs have a significant impact on the absorbed dose of the testes. However, comprehensive studies addressing the effect of organ position on testicular absorbed dose are scarce. Most of the existing research has either relied on simplified phantom models or failed to adequately account for the complex interactions between organs and radiation. This study aims to address this gap by investigating the impact of organ position and surrounding tissues on testicular absorbed dose using Monte Carlo simulations and the Digimouse phantom.

The use of computational phantoms has significantly advanced radiation dosimetry, enabling detailed simulations of energy deposition in tissues. Among these, the Digimouse phantom, a digital mouse model derived from high-resolution CT and MRI data, provides an anatomically realistic representation of a small animal, widely used in preclinical studies [1-2]. It details organ segmentation and makes it an ideal tool for Monte Carlo simulations, which are extensively utilized in radiation transport studies [3]. Digimouse has been employed in a variety of scientific applications, such as dosimetric experiments [4-5], fluorescence molecular tomography [6], and bioluminescence and PET imaging simulations [7].

In this study, we employed the Digimouse phantom to model small animal anatomy with high accuracy. Small animal models, such as mice, are widely used in preclinical radiation research to study biological responses to radiation exposure, evaluate dose distribution in radiosensitive organs, and explore new radiation techniques. Understanding radiation dose distribution in small animal models, such as rats and mice, is essential for correlating experimental outcomes with human clinical scenarios [8]. The Digimouse phantom allows for precise simulations of energy deposition and interactions, making it an ideal tool for this purpose. While an anthropomorphic (human) phantom could provide insights more directly applicable to clinical scenarios, our focus was on preclinical studies to establish foundational knowledge about the impact of radiation source position and surrounding tissues on absorbed dose. These findings can serve as a basis for future research involving human phantoms, thereby contributing to the optimization of radiation therapy protocols in clinical settings.

The Geant4 [9-10-11], a Monte Carlo-based simulation toolkit, is widely used for modeling radiation-matter interactions. It accurately simulates photon transport, energy deposition, and dose distribution at both micro- and nanoscale levels [12-13]. Previously, voxel methods were primarily used to model animal phantoms [14], but more recently, mesh methods have been introduced [15]. Specifically, the mesh-based approach in Geant4 allows for flexible modeling of irregular biological structures, such as small animal phantoms, delivering highly accurate simulation results in a shorter time frame [16].

The testes, as highly radiosensitive organs, are critical to studies investigating radiobiological effects and therapy-related side effects [17-18-19]. Accurate radiation dosimetry is vital for understanding energy deposition and its impact on such sensitive tissues in both preclinical and clinical contexts. Nevertheless, current research often overlooks the complex interactions between radiation source positioning, surrounding tissue composition, and energy deposition in small radiosensitive organs like the testes, especially across a wide photon energy spectrum. The novelty of this study lies in its dual-scenario approach, where energy deposition and absorbed dose in mouse testicular tissue were evaluated under two distinct conditions: (1) with all organs in their anatomically accurate positions, simulating a realistic in vivo scenario, and (2) with the testicular tissue modeled in isolation, simulating an in vitro scenario. By comparing these scenarios, we were able to isolate the effects of surrounding tissues, such as their shielding and scattering contributions, and quantify how they influence dose distributions. This approach provides unique insights into the complex interactions between radiation source positions, anatomical structures, and energy-dependent dose modulation mechanisms. This study provides a detailed energy-dependent analysis of these

interactions using the Digimouse phantom and Monte Carlo simulations.

This study employs the Digimouse phantom in conjunction with Geant4 simulations, to provide a detailed evaluation of absorbed dose in mouse testicular tissue across a wide range of photon energies. The results contribute to enhancing dosimetry accuracy, refining radiation therapy protocols, and reducing risks to radiosensitive organs in both preclinical and clinical contexts.

2. Materials and Methods

2.1. Digimouse

Digimouse was developed using co-registered CT and cryosection images from a 28 g male laboratory mouse, with dimensions of 38*99.2*20.8 mm³. The segmented structures include the whole brain, external cerebrum, cerebellum, olfactory bulbs, striatum, medulla, masseter muscles, eyes, lachrymal glands, heart, lungs, liver, stomach, spleen, pancreas, adrenal glands, kidneys, testes, bladder, skeleton, and skin (Figure 1), These segmentations follow the guidelines outlined in ICRP Publication 145. Table 1 presents the specific characteristics of testicular tissue.

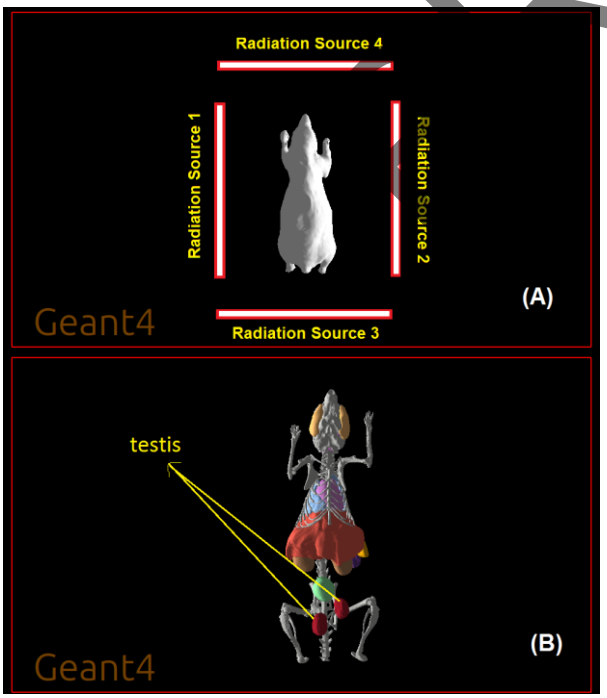

Figure 1. (A) The Digimouse phantom utilized in Geant4 simulations, along with the schematic representation of the radiation source positions. (B) the testis location in this mouse

Table 1. Testicular composites, according to the ICRP 145 publication

Density	1.041 (g/cm³)
Element	**Percent (%)**
H	10.6
C	9.9
N	2.1
O	76.5
Na	0.2
P	0.1
S	0.2
Cl	0.2
K	0.2

2.2. Phantom and Source Modeling in Geant4

This work utilized a 40-core Intel Xeon processor for Geant4 (11.2.1) simulations. The Monte Carlo simulations employed the Livermore physics list, which is specifically optimized for low-energy photon interactions. A cut-off energy of 1 keV was applied to ensure precise energy deposition calculations, particularly at lower photon energies. The Livermore physics list was used as the package for handling physics processes in the simulations. This choice was made to ensure accurate modeling of energy deposition and scattering effects.

Four identical mono-energetic radiation sources were positioned equidistantly around the mouse phantom at the head, tail, and both sides, 2 cm away, to assess the effect of testicular tissue positioning and the influence of surrounding organs on the absorbed dose. The sources were modeled as planar sources with dimensions of 10 × 2.2 cm to ensure uniform irradiation of the mouse phantom and simulate a realistic and practical radiation setup. These sources emitted photons within the energy range of 2 to 10,000 keV, enabling a comprehensive evaluation of energy deposition under various conditions. This configuration ensured uniform irradiation across the mouse phantom to comprehensively evaluate energy deposition. These details are also reflected in Figure 1 (A). For each energy level, a total of 10 million photon beams were simulated. Since the mouse can freely move around the radiation sources in a real laboratory setting, there was no priority in the direction of irradiation. Each source emitted an equal number of

irradiations—10 million beams—resulting in a total of 40 million photon beams per selected source energy.

The deposited energy in the testicular tissue for each irradiation was recorded, and the absorbed dose was calculated by the mass of the testicular tissue. The radiation source energies considered were 2, 5, 10, 15, 20, 25, 35, 50, 100, 200, 500, 1000, 2000, 5000, and 10,000 keV. The absorbed dose unit used in this study was nGy (nanogray). To quantify the precision of the simulation results, the Root Mean Square (RMS) deviation was employed. Also, this study included very low photon energies to comprehensively analyze the energy-dependent behavior of photon interactions with tissue. These low-energy photons were specifically chosen to investigate the dominance of photoelectric absorption and the pronounced shielding effects of surrounding tissues. By examining this range, the study provides insights into dose distribution mechanisms that may be relevant for diagnostic imaging and preclinical research. Understanding the behavior of low-energy interactions highlights the critical role of tissue composition and geometry in dose modulation, especially in radiosensitive organs such as the testes. These findings enhance our understanding of radiation shielding and energy transfer mechanisms, providing valuable insights for future dosimetry studies.

In experimental research, both in vivo and in vitro methods are commonly employed. The key distinction between these approaches lies in their complexity: in vivo methods capture the complete biological interactions within living systems, including those between tissues and organs, whereas in vitro methods are limited to isolated components and lack such systemic interactions.

Drawing on this experimental approach, this study evaluated energy deposition and absorbed dose in mouse testicular tissue under two distinct conditions: (1) with all organs in their anatomically accurate positions and (2) with only the testicular tissue modeled, excluding other organs, under identical irradiation configurations. In the first scenario, the entire mouse body, including all organs, was modeled, and energy deposition and absorbed dose within the testicular tissue were measured. In the second scenario, the testicular tissue was simulated in isolation, and identical irradiation configurations were applied in addition to determining the deposited energy and absorbed dose. The comparison between these two steps highlights the influence of surrounding organs and tissues on the absorbed dose in the testicular tissue.

The mesh method was employed to calculate the absorbed dose in organ-specific geometries using Geant4. The CADMesh library was utilized to import high-resolution 3D models of organs, defined as logical volumes for simulation. Unlike voxel-based methods, which represent space as volumetric pixels, the mesh method uses vertices, edges, and faces to define complex 3D structures. This approach offers high anatomical accuracy and computational efficiency, making it particularly advantageous for modeling small or irregularly shaped organs, such as the testis. Energy deposition was calculated across the entire volume of each organ, and the absorbed dose was obtained over its mass.

While the mesh-based approach offers significant benefits, it is important to note that its accuracy can depend on the resolution of the mesh. Higher-resolution meshes provide greater anatomical detail but may increase computational demands. For this study, high-resolution 3D models were used to ensure accurate geometry while maintaining computational efficiency. Additionally, the statistical nature of Monte Carlo simulations introduces some variability in results, which was minimized by employing a sufficiently high number of photon histories and quantifying uncertainties using the root mean square (RMS) deviation.

3. Results

3.1. Impact of Source Position on Energy Deposition

The energy deposition (MeV) profile in mouse testicular tissue, considering only the testis without the presence of other organs is shown in Figure 2. This profile reveals two prominent peaks corresponding to a dominant photon interaction mechanism at specific energy ranges. The first peak, observed at lower photon energies (approximately 10–50 keV), is attributed to the photoelectric effect, where photons are fully absorbed, resulting in substantial local energy deposition. The second peak, occurring at higher photon energies (above 1 MeV), corresponds to the

onset of pair production, where photons interact with the nuclear field to produce electron-positron pairs, leading to increased energy deposition. In the intermediate energy range (50 keV–1 MeV), Compton scattering dominates, leading to lower energy deposition as photons transfer only a fraction of their energy to electrons. As illustrated in Figure 2, the absence of surrounding organs results in no significant variations in the deposited energy across the four irradiation sources. For all four source orientations, both peaks appear at identical energies. Thus, without the influence of neighboring organs, the impact of testicular location on the deposited energy is negligible (<0.06).

Figure 3 depicts the deposited energy in testicular tissue with the presence of surrounding organs. Compared to Figure 2, the two photoelectric peaks and pair production are still present, but with notable differences. In this case, the absorbed dose varies significantly between opposing sources. Specifically, there is a 29% difference between the left and right sources and a 92% between the tail and head sources. Additionally, for the head source (Source 3), the second peak occurs at higher energies due to the greater distance from the testicle and the presence of additional organs between the source and the testicular tissue. Unlike Figure 2, the peaks are no longer identical across all four sources and are shifted towards higher photon energies.

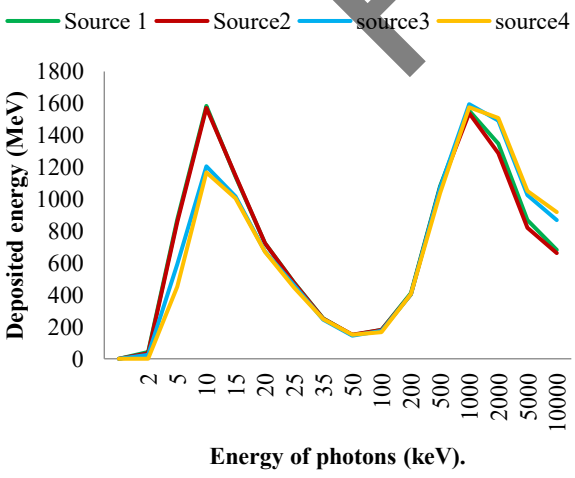

Figure 3. Energy deposition in testicular tissue as a function of photon energy, considering only the testis without surrounding organs

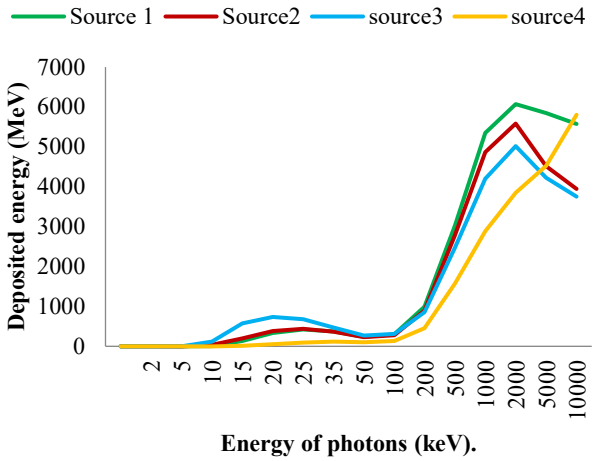

Figure 2. Energy deposition in testicular tissue as a function of photon energy, considering the presence of surrounding organs

3.2. Impact of Surrounding Tissues on Absorbed Dose

In a laboratory environment, mice can freely rotate without a fixed orientation. As a result, the contributions from all four radiation sources were assumed to be equal, and the deposited energy and absorbed dose were calculated for each radiation source. Unlike the previous subsection, which examined the effects of the radiation source position and beam energy on deposited energy, this section specifically focuses on the impact of surrounding organs on the total deposited energy and absorbed dose across various energy levels.

The total deposited energy and absorbed dose in testicular tissue, shown in Figure 4 and Figure 5, exhibit significant variation depending on whether only the testis is considered or if surrounding organs are included. For photon energies below 25 keV, surrounding organs act as a protective shield, absorbing or scattering photons before they can reach the testes, thereby reducing both energy deposition and the absorbed dose. However, for photon energies above 25 keV, secondary scattering effects from neighboring organs enhance the energy deposition and the absorbed dose, with the graph peaks shifting toward higher radiation energies. Interestingly, at 25 keV, the presence or absence of surrounding organs has little to no impact on the absorbed dose in testicular tissue.

The absorbed dose calculations demonstrated high precision, with relative statistical uncertainties consistently below 1.4% across all dosimetric data. This ensures the robustness and reliability of the simulation results under the investigated conditions.

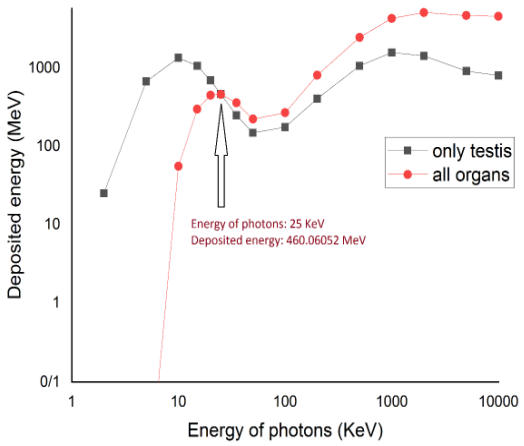

Figure 4. Energy deposition (MeV) in testicular tissue for various photon energies. The blue curve represents only testicular tissue, while the red curve includes all the organs of the mouse

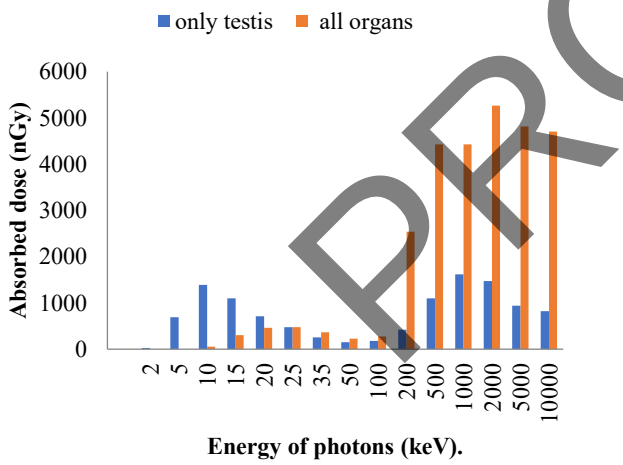

Figure 5. Absorbed dose (nGy) in testicular tissue for various photon energies. The blue bars represent only testicular tissue, while the red bars include all mouse organs

4. Discussion

The simulation results of this work align with trends observed in previous studies that investigated energy deposition in small, radiosensitive organs using Monte Carlo methods. For instance, prior studies have demonstrated that photon energy [20] and surrounding tissues [21] significantly influence dose distributions, consistent with our findings of energy-dependent shielding and scattering effects caused by surrounding tissues. Johnstone and Magdalena [22] emphasized the importance of detailed dosimetry in small-animal phantoms, which validates our selection of the Digimouse phantom for preclinical modeling. Additionally, computational studies on lung cancer radiotherapy [23] have shown that surrounding organs significantly affect dose distributions, and these dose distributions may lead to unexpected toxicities [24], highlighting the importance of considering anatomical structures for accurate dose estimation.

This study provides a comprehensive analysis of energy deposition and absorbed dose in mouse testicular tissue across various radiation energy levels, with and without the inclusion of surrounding organs.

The observed energy deposition patterns are consistent with established photon-matter interaction theories: photoelectric absorption dominates at lower energies, Compton scattering prevails at intermediate energies, and pair production becomes significant at higher photon energies [25-26]. When considering only the testis tissue, the energy deposition profile exhibited two distinct peaks that remained consistent across all source positions, indicating a minimal influence of testicular location on the absorbed dose under such simplified conditions.

However, the inclusion of surrounding organs introduced significant dose variations due to shielding effects at lower photon energies and secondary scattering effects at higher photon energies. These interactions resulted in dose differences of up to 92% between opposing sources and shifted the energy deposition peaks toward higher photon energies. The results demonstrate that total energy deposition is strongly influenced by tissue composition, geometry, and the presence of surrounding anatomical structures. This highlights the necessity of incorporating realistic anatomical features in dosimetric simulations, as simplified models that exclude neighboring tissues may overlook critical dose variations caused by scattering and screening effects, potentially leading to inaccuracies in radiation risk assessment or therapeutic planning.

While this study provides valuable insights into the influence of anatomical structures on energy

deposition, several limitations should be acknowledged. First, the use of the Digimouse phantom, while well-suited for preclinical modeling, may not fully capture the anatomical and compositional complexities of human tissues. Second, the simulations did not include experimental validation due to practical constraints, which limits the ability to confirm the computational findings directly.

Future research should address the current limitations by expanding the study to human phantoms, enabling a direct comparison of absorbed dose differences between humans and small-animal models under the same irradiation conditions. This would provide more actionable insights for translating preclinical findings into clinical applications. Furthermore, experimental validation using physical phantoms or in vivo measurements could enhance the reliability of the results and establish benchmarks for computational models. Also, while this study employed the mesh-based Geant4 approach with the Livermore physics list to model radiation interactions, future research could explore benchmarking the results against other Monte Carlo simulation toolkits or physics libraries, such as Penelope. Comparing trends observed in this study with those derived from alternative methods would not only validate the computational approach but also enhance its robustness for broader applications. Additionally, investigating the effects of different radiation sources and tissue compositions across a wider energy spectrum could improve the generalizability of the findings, ensuring their relevance to diverse clinical and research scenarios.

5. Conclusion

This study examined the effect of radiation source positioning and surrounding tissues on energy deposition and absorbed dose in the radiosensitive testis using Monte Carlo simulations with the Digimouse phantom. Two scenarios were analyzed: (1) with all organs in their accurate anatomical positions and (2) with the testes modeled in isolation, allowing for the quantification of shielding and scattering effects from surrounding tissues. The results underscore the need to consider anatomical structures and photon energy levels in dosimetry for small organs. Our findings enhance preclinical experimental setups and offer insights for improving radiation therapy planning by reducing exposure to healthy tissues while ensuring effective dose delivery to target areas.

Future work will focus on using anthropomorphic (human) phantoms to compare absorbed dose differences between preclinical and clinical contexts, particularly in radiosensitive organs like the testis. This comparison will enhance the translational relevance of our findings and help bridge the gap between preclinical and clinical research. Additionally, experimental validation with physical phantoms or biological tissues will strengthen the reliability of our simulations. Expanding the methodology to other organs and exploring different irradiation configurations will further enhance the applicability of our approach.

References

1- B. Dogdas, *et al.*, "Digimouse: a 3D whole body mouse atlas from CT and cryosection data," *Physics in Medicine & Biology*, vol. 52, no. 3, p. 577, (2007).

2- D. Stout, *et al.*, "Creating a whole body digital mouse atlas with PET, CT and cryosection images," *Molecular Imaging and Biology*, vol. 4, no. 4, p. S27, (2002).

3- R. Yerrou, *et al.*, "Evaluation of the InterDosi code in estimating S-values with the Digimouse voxelized mouse phantom," *Radiation Physics and Chemistry*, vol. 222, p. 111859, (2024).

4- B. M. Mendes *et al.*, "Development of a mouse computational model for MCNPX based on Digimouse® images and dosimetric assays," *Brazilian Journal of Pharmaceutical Sciences*, vol. 53, no. 1, p. e16092, (2017).

5- K. Laazouzi, *et al.*, "Development and validation of a comprehensive S-value database for small animal internal dosimetry in nuclear medicine using the DM_Bra mouse phantom," *Radiation Measurements*, vol. 178, p. 107277, (2024).

6- M. N. Polatoglu *et al.*, "Simulation of fluorescence molecular tomography using a registered digital mouse atlas," in *European Conference on Biomedical Optics*, p. 11074_11, (2019).

7- J. Perens, *et al.*, "An optimized mouse brain atlas for automated mapping and quantification of neuronal activity using iDISCO+ and light sheet fluorescence microscopy," *Neuroinformatics*, vol. 19, no. 3, pp. 433–446, (2021).

8- T. Tolvanen, *et al.*, "Biodistribution and radiation dosimetry of [11C] choline: a comparison between rat and

human data," *European Journal of Nuclear Medicine and Molecular Imaging*, vol. 37, pp. 874–883, (2010).

9- S. Agostinelli, *et al.*, "Geant4—a simulation toolkit," *Nuclear Instruments and Methods in Physics Research Section A: Accelerators, Spectrometers, Detectors and Associated Equipment*, vol. 506, no. 3, pp. 250–303, (2003).

10- J. Allison, *et al.*, "Geant4 developments and applications," *IEEE Transactions on Nuclear Science*, vol. 53, no. 1, pp. 270–278, (2006).

11- J. Allison, *et al.*, "Recent developments in Geant4," *Nuclear Instruments and Methods in Physics Research Section A: Accelerators, Spectrometers, Detectors and Associated Equipment*, vol. 835, pp. 186–225, (2016).

12- M. Jalili Torkamani, *et al.*, "Simulation of energy absorption and dose of ionizing radiation on spike of SARS-CoV-2 and comparing it with human mortality statistics, using Geant4-DNA toolkit," *The European Physical Journal Plus*, vol. 139, no. 1, p. 103, (2024).

13- Y. Heydarizade, *et al.*, "Investigating the possibility of using metamaterial as neutron shield in BNCT treatment to reduce the dose of secondary particles and radioactive elements produced in brain tumor," *Frontiers in Biomedical Technologies*, (2024).

14- A. Mechelli, *et al.*, "Voxel-based morphometry of the human brain: methods and applications," *Current Medical Imaging*, vol. 1, no. 2, pp. 105–113, (2005).

15- A. M. Alshamy, *et al.*, "Study of the reduction of neutron flux through the iron material using GEANT4 simulations," *Journal of Computational and Theoretical Transport*, pp. 1–10, (2024).

16- M. C. Han, *et al.*, "DagSolid: a new Geant4 solid class for fast simulation in polygon-mesh geometry," *Physics in Medicine & Biology*, vol. 58, no. 13, p. 4595, (2013).

17- I. Georgakopoulos, *et al.*, "Radiotherapy and testicular function: A comprehensive review of the radiation-induced effects with an emphasis on spermatogenesis," *Biomedicines*, vol. 12, no. 7, (2024).

18- G. S. Gupta and S. R. Bawa, "Radiation effects on rat testes," *Reproduction*, vol. 44, no. 2, pp. 223–233, (1975).

19- M. L. Meistrich and M. E. A. B. Van Beek, "Radiation sensitivity of the human testis," in *Advances in Radiation Biology*, vol. 14, pp. 227–268, (1990), Elsevier.

20- M. Radwan, *et al.* "The influence of photon energy on dose distribution for IMRT and VMAT plans." *Nowotwory. Journal of Oncology* vol. 64, no. 3, pp. 230-236 (2014).

21- M. Ghorbani, *et al.* "Effect of tissue composition on dose distribution in brachytherapy with various photon emitting sources." *Journal of contemporary brachytherapy,* vol. 6, no. 1, pp. 54-67, (2014),

22- C. D. Johnstone, and B-C. Magdalena. "A review of small animal dosimetry techniques: image-guided and spatially fractionated therapy." *Journal of Physics: Conference Series*. Vol. 2630, No. 1, (2023), IOP Publishing.

23- J.L. Thalhofer, *et al.* "Equivalent dose calculation in simulation of lung cancer treatment and analysis of dose distribution profile." *Applied Radiation and Isotopes*, vol. 142, pp. 227-233, (2018) Elsevier.

24- R. B. Sparks, *et al.* "Radiation dose distributions in normal tissue adjacent to tumors containing 131I or 90Y: the potential for toxicity." *Journal of Nuclear Medicine* vol. 43, No. 8, pp. 1110-1114, (2002) Soc Nuclear Med.

25- G. Keiser, "Light-tissue interactions," Biophotonics: Concepts to Applications, pp. 147–196, (2016), Springer.

26-B. J. McParland, "Photon interactions with matter," *Nuclear Medicine Radiation Dosimetry: Advanced Theoretical Principles*, pp. 171–207, (2010), Springer